12-1-2010

Sympathetic neural activation: An ordered affair

Craig D. Steinback
Western University

Aryan Salmanpour
Western University

Toni Breskovic
Medicinski Fakultet, Sveuciliste u Splitu

Zeljko Dujic
Medicinski Fakultet, Sveuciliste u Splitu

J. Kevin Shoemaker
Western University, kshoemak@uwo.ca

Sympathetic neural activation: an ordered affair

Craig D. Steinback[1], Aryan Salmanpour[1,2], Toni Breskovic[3], Zeljko Dujic[3] and J. Kevin Shoemaker[1,4]

[1]*Neurovascular Research Laboratory, School of Kinesiology, University of Western Ontario, London, Ontario, Canada*
[2]*Department of Electrical and Computer Engineering, University of Western Ontario, London, Ontario, Canada*
[3]*Department of Physiology, University of Split School of Medicine, Soltanska 2, 21000 Split, Croatia*
[4]*Department of Physiology and Pharmacology, University of Western Ontario, London, Ontario, Canada*

Is there an ordered pattern in the recruitment of postganglionic sympathetic neurones? Using new multi-unit action potential detection and analysis techniques we sought to determine whether the activation of sympathetic vasomotor neurones during stress is governed by the size principle of recruitment. Multi-unit postganglionic sympathetic activity (fibular nerve) was collected from five male subjects at rest and during periods of elevated sympathetic stress (end-inspiratory apnoeas; 178 ± 37 s(mean ± S.D.)). Compared to baseline (0.24 ± 0.04 V), periods of elevated stress resulted in augmented sympathetic burst size (1.34 ± 0.38 V, $P < 0.05$). Increased burst size was directly related to both the number of action potentials within a multi-unit burst of postganglionic sympathetic activity ($r = 0.88 \pm 0.04$, $P < 0.001$ in all subjects), and the amplitude of detected action potentials ($r = 0.88 \pm 0.06$, $P < 0.001$ in all subjects). The recruitment of larger, otherwise silent, neurons accounted for approximately 74% of the increase in detected action potentials across burst sizes. Further, action potential conduction velocities (inverse of latencies) were increased as a function of action potential size ($R^2 = 0.936$, $P = 0.001$). As axon diameter is positively correlated with action potential size and conduction velocity, these data suggest that the principle of ordered recruitment based on neuronal size applies to postganglionic sympathetic vasomotor neurones. This information may be pertinent to our understanding of reflex-specific recruitment strategies in postganglionic sympathetic nerves, patterns of vasomotor control during stress, and the malleability of sympathetic neuronal properties and recruitment in health and disease.

(Received 5 July 2010; accepted after revision 7 October 2010; first published online 11 October 2010)
Corresponding author J. K. Shoemaker: Neurovascular Research Laboratory, School of Kinesiology, Room 3110, Thames Hall, University of Western Ontario, London, ON, Canada, N6A 3K7. Email: kshoemak@uwo.ca

Abbreviations CWT, continuous wavelet transform; HbSat, arterial haemoglobin saturation; HR, heart rate; MAP, mean arterial pressure; MSNA, muscle sympathetic nerve activity; SNR, signal to noise ratio; TPR, total peripheral resistance.

Introduction

Sympathetic activity controlling the vasomotor tone of blood vessels within skeletal muscle occurs in an irregular pattern of spontaneous 'bursts' of action potentials that are synchronous with the cardiac cycle and can be assessed using the technique of microneurography (Wallin, 1993). Due to an inherently low signal-to-noise ratio, as well as the variable impact of electrode proximity in relation to populations of postganglionic sympathetic neurones, recorded sympathetic activity is typically rectified and integrated to give peaks of activity quantified in terms of burst frequency, burst probability (bursts per 100 heart beats), or relative integrated burst size that is, in turn, related to the number of action potentials that occur within the burst. However, information about the firing characteristics of individual sympathetic neurones is lost with this approach. Nonetheless, the behaviour of these integrated bursts has led to hypotheses regarding neuronal recruitment strategies. For example, the observation that larger bursts typically have a shorter conduction latency indicates that (1) synaptic delays within sympathetic reflex arcs can be modified so that neurones are recruited earlier in the cardiac cycle, and/or (2) that a latent population of neurones exists that have a faster conduction velocity such that their signal contributes to the integrated output earlier (Wallin *et al.* 1994; Xie *et al.* 1999). These hypotheses have remained untested due to limitations in extracting action potential information from the noisy neurogram.

An important advance in studying sympathetic neural firing patterns was made by Macefield and colleagues who

DOI: 10.1113/jphysiol.2010.195941

adapted methods originally used to detect and record activity from single motor and sensory neurones to the study of single sympathetic neurones (Macefield *et al.* 1994). Data from these authors (Macefield *et al.* 1994, 1999; Macefield & Wallin, 1999; Ashley *et al.* 2010) and others (Lambert *et al.* 2007) demonstrates that, at rest, a given sympathetic vasomotor neurone fires in approximately 61% of detected bursts of activity (range 43–100%). Further, when active, sympathetic neurones fire predominately once within a given burst of activity (~70% of occurrences) (Macefield *et al.* 1994; Macefield & Wallin, 1999) with multiple firings of the same neurone within a burst increasing during voluntary apnoea (Macefield & Wallin, 1999) and with certain pathologies (Elam *et al.* 2002). To date, information regarding the population of neurones available for recruitment in the postganglionic sympathetic activity, or the recruitment of additional higher-threshold neurones during progressive sympathetic activation is very limited. Though Tsukahara & Mano (1997) suggest evidence of a hierarchal pattern of recruitment in single vasoconstrictor neurones correlated to R-R interval and inversely related to prevailing diastolic blood pressure, the neuronal properties governing such a recruitment pattern remain unknown.

An analogous comparison of potential recruitment properties of postganglionic sympathetic neurones may be drawn from what is known about motor-neurone firing patterns. The firing and recruitment pattern of skeletal muscle motor neurones during motor tasks follows Henneman's size principle whereby smaller motor neurones with slower conduction velocity are recruited first with larger, higher threshold, neurones being recruited under increasing load (Henneman *et al.* 1965). Once recruited, the firing rates of active neurones increase (Westgaard & De Luca, 2001). Thus, both rate coding and ordered recruitment based on neuronal size are mechanisms used to regulate muscle activation. Whether the sympathetic nervous system operates on similar principles remains unknown.

To address this question, our laboratory has developed a technique that enables the identification and morphological classification of multiple vasomotor neurones contributing to sympathetic bursts (Salmanpour *et al.* 2010). Using this approach we tested the hypothesis that reflex augmentation of sympathetic vasomotor activity is characterized by the successive recruitment of higher threshold sympathetic vasomotor neurones. Our approach was to generate a large range of sympathetic outflow and examine the rate, size and latency of action potentials. Chemoreflex stress has been shown to affect both the size and frequency of integrated bursts (Malpas *et al.* 1996; Steinback *et al.* 2009). Further, the cessation of breathing also augments the sympathetic response to chemoreflex stress. Thus, to produce a large number of sympathetic bursts under severe chemoreflex stress in human recordings, we took advantage of the ability of trained free divers to perform prolonged breath holds and, thereby, both generate and sustain high levels of sympathetic activity for analysis.

Methods

Subjects

Five healthy, males (24 ± 1 years, 185 ± 8 cm, 85 ± 7 kg, means $\pm$ S.D.) participated in this study after receiving verbal and written instructions outlining the experimental procedures and having providing informed written consent. All participants were non-smokers and none had any history of cardiovascular or respiratory disease. Participants arrived at the lab at least 2 h postprandial and having abstained from caffeine, alcohol or other stimulants for 12 h. Participants voided their bladder immediately prior to testing. The study was performed at the University of Split, Croatia in order to obtain data in trained free divers. The protocol was approved by both the Health Sciences Research Ethics Board at The University of Western Ontario in Canada and the research ethics board at The University of Split School of Medicine in Croatia.

Experimental protocol

Data were collected during a 5 min period of rest (spontaneous breathing) and during a maximal, end-inspiratory, breath-hold. End-inspiratory breath-holding causes (1) a reduction in venous return and cardiac output, both of which will cause baroreceptor unloading, and (2) combined hypoxia and hypercapnia. These combined stimuli cause marked increases in sympathetic efferent activity. Participants were encouraged to continue breath-holding as long as they could endure in order to maximize sympathetic activation. Average breath-hold duration was 178 ± 37 s, causing a $10 \pm 3\%$ decrease in arterial oxygen saturation (Poet II, Criticare Systems, Waukesha, WI, USA) and a $40 \pm 11\%$ decrease (nadir) in cardiac output (Finometer; Finapres Medical Systems, Amsterdam, The Netherlands).

Mean arterial blood pressure was observed on a beat-by-beat basis from the blood pressure waveform using finger photoplethysmography (Finometer; Finapres Medical Systems). Heart rate was calculated from a standard electrocardiogram.

Sympathetic neural recordings

Muscle sympathetic nerve activity (MSNA) was assessed in the right fibular (peroneal) nerve by microneurography (Hagbarth & Vallbo, 1968). A tungsten microelectrode (35 mm long, 200 μm in diameter, and tapered to a

1–5 μm uninsulated tip) was inserted percutaneously into the fibular nerve posterior to the fibular head. A reference electrode was positioned subcutaneously 1–3 cm from the recording site. A suitable sympathetic nerve site was searched for by manually manipulating the microelectrode until a characteristic pulse-synchronous burst pattern was observed. Confirmation that the recorded signal represented MSNA was determined by the absence of skin paresthesia and a signal that increased in response to voluntary apnoea but not during arousal to a loud noise (Delius *et al.* 1972). The MSNA neurogram was amplified 1000× through a pre-amplifier and 100× by a variable-gain, isolated amplifier. The amplified, raw MSNA signal was band-pass filtered at a bandwidth of 700–2000 Hz, sampled at 10,000 Hz and stored offline for further analysis (Powerlab software, ADInstruments Inc., Colorado Springs, CO, USA). Previous work from our laboratory (unpublished) indicates that the band-pass filter settings applied to the raw data do not impair our ability to detect action potential waveforms. However, the impact of signal conditioning, including amplifier characteristics and band-pass filter settings, on AP morphology requires further assessment.

Integrated bursts of MSNA were identified as exhibiting pulse synchrony, having a signal-to-noise ratio of least 2:1 with respect to the previous period of neural silence between bursts, having characteristic rising and falling slopes, and increasing in incidence and size during end-expiratory apnoeas but not startle. Burst occurrence was confirmed by visually inspecting the corresponding raw neurogram.

Action potential detection and analysis

Action potentials were detected and extracted from the filtered raw MSNA signal using the techniques developed in our laboratory by Salmanpour *et al.* (2010). Briefly, this technique used a continuous wavelet transform (CWT) for action potential detection. The CWT used a 'mother wavelet' that was adapted to an average action potential waveform constructed from (and hence with the same morphology as) physiological recordings of post-ganglionic sympathetic action potentials (Salmanpour *et al.* 2010). The CWT was in turn applied to the filtered MSNA to provide a wavelet coefficient between the signal of interest (i.e. an action potential) and the mother wavelet such that the wavelet coefficient was largest in the presence of the action potentials and negligible when applied to noise. Wavelet coefficients related to action potentials and noise were separated based on thresholding analysis (Johnstone & Silverman, 1997). The exact location of the negative peak for each action potential was then detected by isolating the largest supra-threshold wavelet coefficient. Using this location information the action potential waveforms were obtained from the original filtered raw signal by putting the estimated location of action potentials in the centre of a predefined window (3.2 ms). In this way, the amplitude and morphology of each extracted action potential remained unaltered. Extracted action potentials were then ordered based on peak-to-peak amplitude, and histogram analysis was performed to separate action potentials into amplitude-based clusters. Cluster bin widths were automatically defined based on Scott's rule which balanced bin width, data bias and variance to minimize the integrated mean square error (Scott, 1979). As such, the number of total clusters varied by subject.

The signal-to-noise ratio for a period of data was determined as the amplitude of the negative peak of the mean action potential over the standard deviation of the background noise (i.e. during sympathetic silence).

The latency of individual action potentials was determined as the time between the R-wave of the preceding cardiac cycle and the negative peak of the action potential waveform, similar to that described previously (Fagius & Wallin, 1980).

Action potential summation simulation

Using published data from recordings of single post-ganglionic sympathetic axons (Macefield & Wallin, 1999), a simulation analysis was performed to determine the probability of action potential overlap. From these previous data, we assumed each neurone was active only once within a burst of activity, had a mean firing frequency of 0.33 Hz, and had a firing probability (percentage of heart beats during which a neurone was active) of 35%. The shape and amplitude of each action potential was the same between 'neurones' and the duration was fixed at 3.2 ms. A population of 30 simulated 'neurones' was used for this simulation. Each 'neurone' was active independently from the others. Using these criteria, 10,000,000 simulated bursts of sympathetic activity were generated. These data were then assessed for overlapping action potentials ($<$0.3 ms separation).

Two possible patterns of summation were expected. First, complete superimposition would produce a larger than expected action potential that would occupy a bin that was not contiguous in the binning designation. Second, incomplete summation would produce an aberrant waveform whose shape and amplitude would be misleading but, nonetheless, composed of two action potentials that could be counted. Thus, action potential clusters were eliminated if they were larger than all others and in a bin that was not contiguous with the remaining data. Further, action potential waveforms that were not tri-phasic and of small amplitude were also eliminated from the analysis.

Statistical analysis

All statistical analyses were performed using SigmaStat 3.11 (Systat Software Inc., San Jose, CA, USA). Differences between baseline and maximal activation during breath-holding were assessed using Student's two-tailed, paired *t* test. Where multiple comparisons were performed, *P* values were corrected using the comparison-wise error rate (α, 0.05) and the calculated family-wise error rate (α_f) as described by Hinkle *et al.* (2003):

$$P^1 = \alpha(P^0/\alpha^1)$$
$$\alpha^1 = \alpha_f/c$$
$$\alpha_f = 1 - (1-\alpha)^c$$

where P^0 and P^1 represent the original and corrected *P* values respectively, α^1 is the adjustment factor based on the chosen level of significance and *c* represents the number of comparisons made.

The relationship between the number of action potentials and action potential clusters within a burst was quantified by Pearson's correlation analysis. Data are expressed as means ± S.D. with significance set at $P < 0.05$.

Results

At rest, subjects exhibited typical integrated post-ganglionic neural activity (13 ± 5 bursts min^{-1}; 20 ± 7 bursts per 100 heart beats) with a mean reflex burst latency of 1.34 ± 0.06 s following the R-wave of the preceding cardiac cycle. Subjects subsequently performed breath-holding for a period of 178 ± 37 s. Compared to baseline (0.24 ± 0.04 V; spontaneous breathing), at end breath-hold, integrated sympathetic burst size was increased (1.34 ± 0.38 V, $P < 0.05$) and this increase was inversely related to burst latency (slope $= -0.00033 \pm 0.00014$ s V^{-1}; $r = -0.544 \pm 0.099$, $P < 0.001$ in all cases). The increase in sympathetic nerve activity during breath-holding was associated with a pronounced increase in mean arterial pressure ($P < 0.001$) and total peripheral resistance (Table 1; $P < 0.05$).

For sympathetic action potential analyses, 220 ± 64 integrated sympathetic bursts consisting of a total of 3974 ± 1455 detected action potentials were analysed per subject across the entire protocol (i.e. with spontaneous breathing and during breath-holding). Compared with baseline, breath-holding increased the number of action potentials per integrated burst ($P < 0.001$; Table 2), consistent with the observed increase in integrated burst size. When detected action potentials were binned based on peak-to-peak amplitude. The number of distinct 'clusters' of action potentials was also increased during breath-holding ($P < 0.001$). For an example of detected sympathetic action potential clusters see Fig. 1.

Table 1. Chemoreflex stimuli, integrated sympathetic activity responses, and cardiovascular consequences of breath-holding

	Pre-breath-hold	End breath-hold
HbSat (%)	99 ± 1	80 ± 11*
P_{aCO_2} (Torr)	37.5 ± 4.5	51.0 ± 3.0†
pH	7.44 ± 0.05	7.34 ± 0.04†
Burst size (V)	0.24 ± 0.04	1.34 ± 0.38*
HR (bpm)	65 ± 10	60 ± 9
MAP (mmHg)	102 ± 21	134 ± 13†
$\dot{Q}$ (l min^{-1})	7.3 ± 2.1	6.8 ± 1.8
TPR (mmHg l^{-1} min^{-1})	11.8 ± 1.7	20.8 ± 6.3*

Values expressed as means ± S.D. HbSat, arterial haemoglobin saturation; P_{aCO_2}, arterial partial pressure of carbon dioxide; HR, heart rate; MAP, mean arterial pressure; $\dot{Q}$, cardiac output; TPR, total peripheral resistance. †Significantly difference from pre-breath-holding, $P < 0.001$; *significantly different from pre-breath-holding, $P < 0.05$.

Regression analysis demonstrated the strong relationship between integrated burst size and the number of action potentials ($r = 0.88 \pm 0.04$, $P < 0.001$ in all subjects) as well as action potential clusters ($r = 0.88 \pm 0.06$, $P < 0.001$ in all subjects). Further, the number of detected action potentials and the number of unique clusters within a given burst of sympathetic activity were strongly correlated ($r = 0.9 \pm 0.06$, $P < 0.001$ over all subjects) with the recruitment of additional clusters accounting for approximately 74% of the increase in detected action potentials across burst sizes (Fig. 2). Thus, the remaining, unexplained, increase in action potential content with increasing integrated burst size was likely to have been a function of increased action potential firing frequency. Figure 3 shows the relationship between the occurrence of individual action potential clusters as a function of burst amplitude in subjects with low and high signal-to-noise ratios.

The latency of individual action potentials with respect to the preceding R-wave of the ECG was taken to represent an inverse index of neural conduction velocity. This latency was used to determine if recruited action potential clusters represented faster conducting, and in turn larger, neurones. Action potential cluster latency decreased in each participant as a function of peak-to-peak amplitude, with the mean response fitting an exponential decay pattern ($R^2 = 0.936$, $P = 0.001$) consistent with the known relationship between action potential amplitude, the square of axon diameter, and conduction velocity (Clamann & Henneman, 1976) (Fig. 4).

Simulation analysis was performed to determine the possible effect of action potential summation (i.e. two action potentials firing at exactly the same time to produce

Table 2. Postganglionic sympathetic action potentials and action potential clusters detected at rest and during maximal breath-holding for each participant

	Baseline		Maximal activity		
Subject	Action potentials/burst	Active clusters/burst	Action potentials/burst	Active clusters/burst	Total detected clusters
1	19	6	46	12	14
2	7	3	37	12	16
3	23	6	54	16	24
4	13	4	39	14	22
5	8	3	23	9	11
Mean ± S.D.	14 ± 7	4 ± 2	40 ± 12*	13 ± 3*	17 ± 5†

Total detected clusters indicate the number of clusters identified throughout the entire protocol. The difference between the total detected clusters and the number of clusters present during maximal activity at the end of breath-holding indicates that not all clusters are recruited at one time. *Significantly different from baseline, $P < 0.01$. †Significantly different from action potential clusters per burst during maximal activity, $P < 0.05$.

a summated action potential waveform) within larger bursts of activity. A simulated population of 30 'neurones' was used to create bursts of action potential waveforms of moderate amplitude with inter-spike intervals that were assigned based on physiological criteria (i.e. within-burst action potential distribution and neural activity probabilities). After generating 10,000,000 simulated bursts of data (containing 1.2×10^8 simulated action potentials), the probability of 'complete' action potential overlap (action potential separation <0.3 ms) and summation to produce a single, larger amplitude waveform was 0.28%. However, partial separation and overlap between 0.3 ms and 2 ms occurred 3% of the time. Within this range, action potentials with a separation of >0.7 ms could be detected as distinct waveforms and only action potentials with a separation >1.4 ms could be confidently counted and classified further based on amplitude. In addition to capturing the majority of action potentials accurately, this cut-off of 1.4 ms will also capture multiple firings of single units that, in theory, could fire at 500 Hz (every 2 ms) (Grundfest & Gasser, 1938) but, *in vivo*, appear to display maximal instantaneous firing rates of up to 230 Hz (Macefield *et al.* 1994; Macefield & Wallin, 1999).

Discussion

The results of the current study increase our understanding of how the sympathetic nervous system is regulated during reflex activation. Here, we demonstrate the potential for patterned recruitment of previously silent and faster-conducting postganglionic sympathetic neurones. As such, the principle of recruitment based on neuronal size (e.g. Henneman's size principle as observed in the skeletal motor system) appears to be conserved across excitable neural systems. This interpretation is supported by evidence of (1) an increase in the number of action potentials within a given burst of sympathetic activity in relation to integrated burst size (i.e. peak height), (2) the recruitment of otherwise silent clusters of sympathetic neurones as a function of integrated burst size, and most importantly, (3) the increased presence of larger action potentials (axons) during sympathetic excitation elicited by breath-holding.

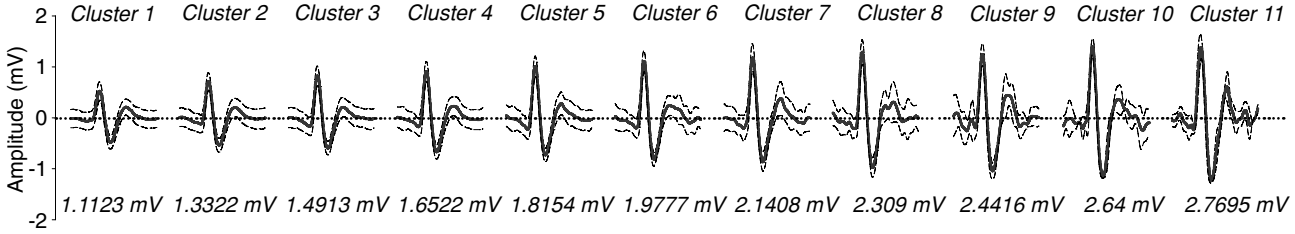

Figure 1. Representation of mean postganglionic sympathetic action potential clusters detected in 189 bursts of MSNA, containing 1777 action potentials in one participant (Subject 5) during rest and breath-holding

Continuous and dashed lines represent means and standard deviations of cluster amplitudes. Clusters are binned based on peak-to-peak amplitude of each action potential (mean amplitude indicated below each cluster).

A consideration of this study is the assumption that larger amplitude action potentials reflect larger neurones. This assumption must be considered carefully, with three mechanisms by which larger amplitude waveforms might appear. First, concurrent firing of neurones could summate producing an erroneously large action potential (Spickler & Kezdi, 1969; Andresen & Yang, 1989). We believe the potential for this scenario to occur

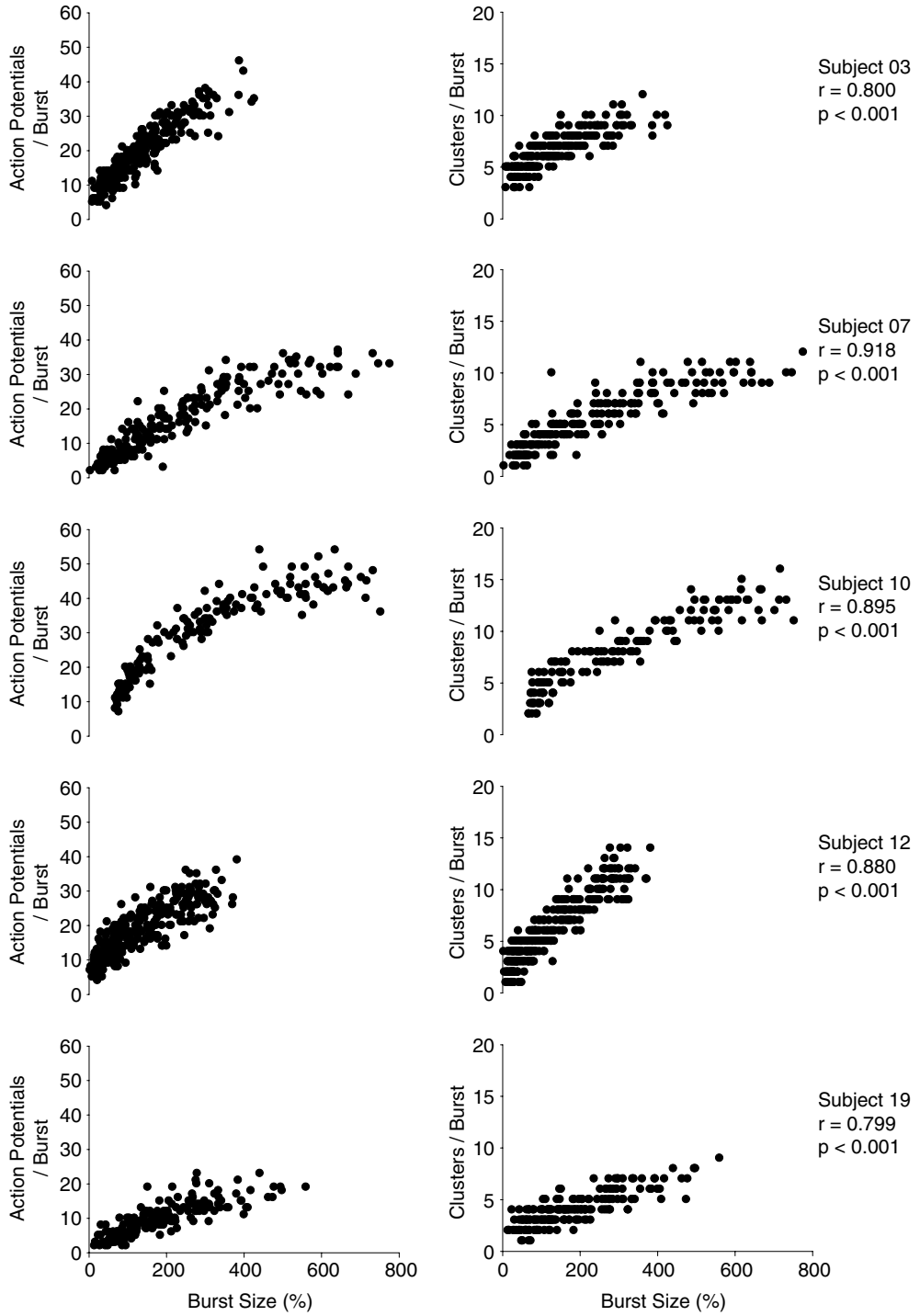

Figure 2. Number of postganglionic sympathetic action potentials and clusters occurring per burst as a function of relative integrated burst size (100% represents mean resting burst size)
R and *P* values represent the correlation between the number of detected action potentials and unique action potential clusters per burst. Between 64 and 84% of the increased action potential content during stress appears to be related to the recruitment of additional clusters.

is minimal for two reasons. (1) Our simulation data suggest that the likelihood of action potential overlap and summation is very low even in the largest bursts of activity, accounting for 3 in 1000 action potentials. As the pattern of recruitment observed is evident across the entire range of burst sizes, including smaller bursts where the number of action potentials and potential for action potential summation will be lower, the impact of this phenomenon on the current data is likely to be minimal. (2) We have demonstrated previously a high accuracy of the analysis

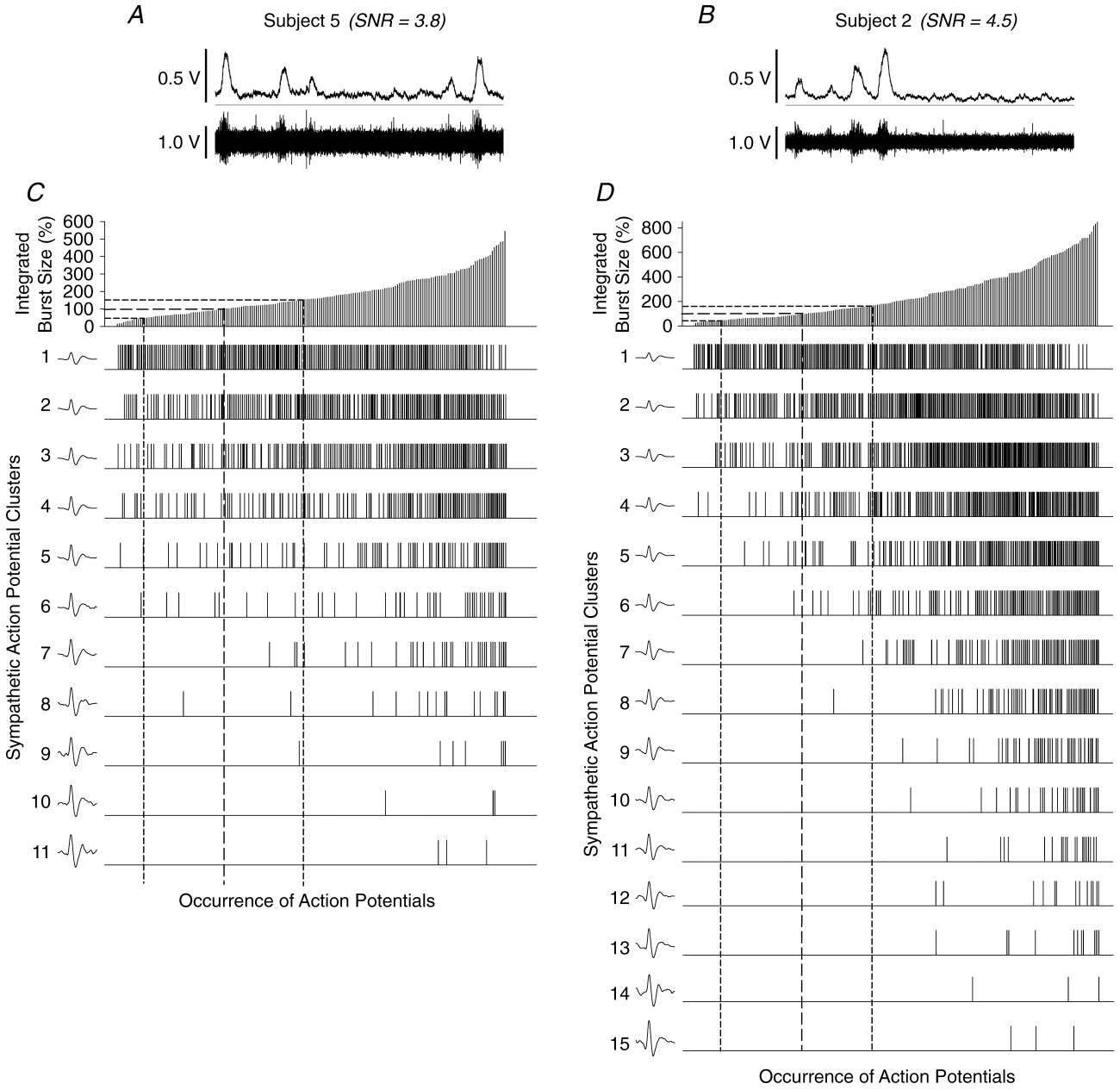

Figure 3. Examples of data obtained from a subject with a low (*A* and *C*) and a subject with a high (*B* and *D*) signal-to-noise ratio

A and *D* illustrate 10 s of the integrated and raw neurograms obtained at baseline from either subject. *C* and *D* illustrate the pattern of action potential occurrence as a function of sympathetic burst size and cluster amplitude, for either subject. Range of integrated sympathetic bursts ordered by burst size as a percentage of baseline (*C* and *D*, top panels). Dashed lines represent the means and standard deviations of integrated burst sizes at baseline. The occurrences of postganglionic sympathetic action potentials as a function of integrated burst size are indicated for each action potential cluster below. Dashed drop lines indicate range corresponding to baseline bursts. In both subjects, clusters of larger amplitude are predominately recruited at higher levels of sympathetic activation (as determined by integrated burst size).

method which reduces the likelihood of false detections (or misses) in a manner that is non-linearly related to the signal-to-noise ratio of the raw neurogram (Salmanpour *et al.* 2010). In the present study, the signal-to-noise ratio for the data ranged from 3.6 to 4.7 (or very high). Based on a previous validation analysis (Salmanpour *et al.* 2010) this level of signal-to-noise would produce a correct detection rate of $93 \pm 7\%$ and a false positive detection rate of $1 \pm 1\%$. Further, any truly overlapping action potentials would result in a summated waveform that is randomly positioned within a burst and thereby less likely to fit the observed size-latency relationship.

A second mechanism by which larger amplitude action potentials might appear is that the amplitude of a given detected action potential is dependent not only on the size of the neurone from which it was generated but also the neurone's proximity to the recording electrode. In this way a small neurone which is close to the electrode may have an apparently equivalent or larger action potential than that of a larger but more distant neurone. As such, we cannot determine for certain the size of neurones corresponding to a particular action potential cluster. Nor can we be certain that any one cluster does not represent numerous neurones with the same detected action potential amplitude. However, it is expected that the receptive field of the electrode will remain constant over time, as will the total number of potential neurones from which a signal is obtained. Thus, any neurone will continue to produce the same amplitude action potential over time and will be binned within the same action potential cluster whenever it is detected. Additionally, the volume of data analysed still demonstrated the pattern expected based on the relationship between action potential size, action potential conduction velocity and, subsequently, axon diameter. Thus, whereas any variations in neurone proximity to the recording electrode will contribute to the variability of the action potential amplitude *versus* latency relationship, this variability does not mask the general pattern. Also, the evidence that the larger action potentials were predominately present in larger bursts during breath-holding argues against a spatial concern. In fact, evidence that single neurones fire in ~21% of cardiac cycles in young healthy individuals (Macefield *et al.* 1994) would argue that if these signals were not based

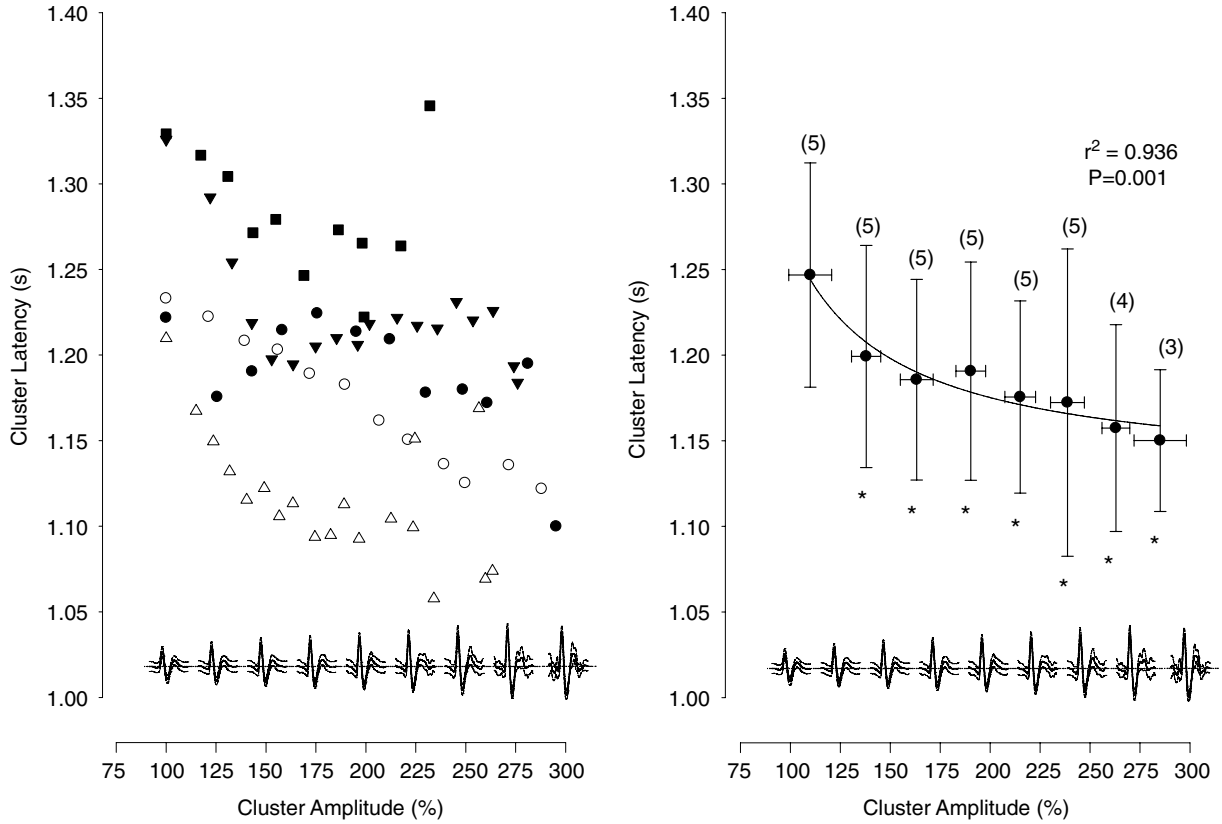

Figure 4. Mean action potential latency from the corresponding R-wave, for each cluster, as a function of normalized cluster amplitude (cluster 1 = 100%; see inset at bottom of each panel) for each participant (left panel)

Mean cluster latency, binned across participants, as a function of normalized cluster amplitude (right panel). Numbers indicate the number of subjects per bin. The decrease in cluster latency as a function of amplitude was fitted with a modified exponential decay (see text). *Latency significantly different from first bin, $P < 0.05$.

on a recruitment order, larger action potentials would be observed randomly over time regardless of burst size; generally, this was not the case.

The third possibility is that different neurones do have varying diameters and that larger neurones produce larger amplitude voltage signals in a pattern of successive activation. Upon exclusion of the previous two possibilities, together with evidence that larger action potentials demonstrated reduced reflex latency, and were generally restricted to the high stress condition, we propose that these clusters of larger action potentials are, indeed, reflective of a latent population of larger diameter sympathetic neurones. Indeed, limited data indicate that c-fibres in excised human nerves express a range of diameters from 0.2 to 2.0 μm (Chad *et al.* 1981; Jacobs & Love, 1985).

In addition to the potential challenges of action potential summation, dealt with above, there is concern about the reliability of the current method to efficiently extract action potentials from a background of Gaussian noise. To address this concern we have performed additional analysis with the approach and results provided in Appendix I, below. The results indicate a high degree of correct detection and low degree of false negative action potentials and indicate that the detection algorithm is highly successful.

A further consideration is that the recorded action potentials tended to have a prominent positive component instead of the singular dominant negative component observed in most (Macefield *et al.* 1994; Lambert *et al.* 2007; Murai *et al.* 2009), but not all (Diedrich *et al.* 2003) reports of extracellular c-fibre recordings. This raises the concern that these action potentials may be of origins other than efferent sympathetic c-fibres. However, this is unlikely for several reasons. (1) Our determination of sympathetic bursts was based on a series of criteria which included pulse synchrony as well as increased burst presence and size in response to an end-expiratory apnoea but not startle. To our knowledge, there is no evidence that muscle spindle occurrence increases during apnoea. (2) The latency value for every action potential measured was $>$1.0 s (consistent with all other reported sympathetic latency values) whereas as the ECG muscle spindle latency reported by McKeon & Burke (1981) is $<$0.5 ms. (3) The general action potential shape depicted in Fig. 1 was consistent across all action potential amplitudes (as shown) as well as across recordings in all participants. If an admixture of action potentials from other non-sympathetic neurons occurred then this admixture must have been present during all recordings with sufficient numbers of action potentials to contribute to a prominent positive component without overtly increasing the standard deviation of the mean waveform.

In the absence of a physiological rationale for the prominent positive aspect of the action potentials reported in this analysis, we believe the hardware used to obtain and condition the neurogram is affecting action potential morphology. Specifically, the pre-amplification, variable gain amplification and application of a band-pass filter have the potential to alter the shape of the recorded action potential. In Appendix II we provide supplemental data that demonstrate this effect. Specifically, this analysis illustrates a recorded sympathetic action potential and the calculation of the morphology of the same action potential after removing the effects of amplification and band-pass filtering that occur with the Iowa Bioengineering nerve traffic analyzer that was used for the current action potential recordings. From this analysis, it is clear that the original action potential (before conditioning) has a dominant negative component.

The pulse-synchrony of sympathetic bursts indicates that their occurrence is under baroreflex regulation whereas variations in burst size appear to be under a different mechanism of control (Kienbaum *et al.* 2001). Wallin *et al.* (1994) documented the inverse relationship between integrated burst size and burst latency. In the absence of action potential information, the authors surmised that these variations in burst latency were due to differences in (1) cardiovascular transmission and sensing by the baroreceptors, (2) baroreceptor afferent conduction time, (3) central processing, or (4) efferent transmission along pre- and postganglionic sympathetic fibres. Thus, understanding the mechanism of augmented burst size is critical for understanding the fundamental central processes involved in sympathetic activation. In a concurrent study, Macefield *et al.* (1994) demonstrated that the action potential latency of a single axon varies over 358 ± 33 ms, suggesting considerable variation of synaptic delays in the baroreflex arc. In contrast, the latency of an action potential in relation to the rest of the activity within a burst exhibited a relatively uniform temporal relationship, compatible with a fixed recruitment order of individual sympathetic neurones (Macefield *et al.* 1994). Thus, these earlier data suggested that synaptic delays applied similarly to all neurones within a burst of sympathetic activity. However, in the current analysis we demonstrate that larger amplitude postganglionic vasoconstrictor neurones are recruited during apnoeic stress and that these have shorter conduction latencies. Therefore, it is likely that both central processing and recruitment of faster conducting neurones play important roles in determining integrated burst latency and total sympathetic activity.

In young and healthy individuals, a sympathetic neurone is active in $\sim$60% of bursts, and when active, fires primarily once within a given burst (Macefield *et al.* 1994; Macefield & Wallin, 1999). This timing appears to be an inherent principle of recruitable neurones. For example, Meckler & Weaver (1988) observed a firing rate of 1.2 action potentials s^{-1} in feline splenic and renal

sympathetic neurones. Also, when Macefield & Elam (2004) constrained α-motor neurones to brief periods of contraction-related bursty activity, a pattern of single firing per burst predominated similar to that observed in bursts of sympathetic activity. For sympathetic bursts the implication is that increased action potential content during heightened sympathetic activation is likely to be due to recruitment of additional neurones as well as repeated firing of the same neurones. Our data are in keeping with this idea in that 74% of the action potentials detected were statistically accounted for by the number of clusters and not by an increased number of action potentials within pre-existing burst clusters. This is directly comparable to ∼70% solitary firing rate described for individual neurones (Macefield *et al.* 1994; Macefield & Wallin, 1999). As such, we advance previous data to provide evidence that sympathetic activation is predominately achieved by recruiting groups of larger neurones. However, though the pattern of recruitment of individual neurons demonstrated here suggests a hierarchal order of activation, some variation in this pattern is obvious (Fig. 3). In particular, the appearance of a new cluster in one burst does not mean it will always be present. A limitation of this approach is that it cannot be determined whether or not the same neurones are active in each burst. Furthermore, the largest bursts, occurring under the most severe sympathetic activation, do not necessarily contain all clusters, although it is more likely that they will. Thus, there is a probabilistic basis of recruitment, similar to that of single units (Macefield *et al.* 1994; Macefield & Wallin, 1999).

There are three potential mechanisms that may explain the observed variations in the expected recruitment order (i.e. larger neurons with larger action potentials being recruited within larger integrated bursts of activity). First, as discussed above, overlap of concurrent two smaller action potentials within a smaller integrated burst of activity may result in a larger compound waveform that does not fit the recruitment pattern. While such waveforms are likely to contribute to this variation, we calculate this contribution of completely overlapping neurones to be quite low (0.3%). Secondly, the signal-to-noise ratio of the recorded signal may affect the rate of false action potential detection. As such, a lower signal-to-noise ratio may be associated with more false detections which do not fit the expected recruitment pattern. However, as indicated above, all recordings used in the current investigation were considered to have high signal-to-noise ratios, with a calculated false detection rate of ∼1%. Finally, the recruitment of individual neurones is the function of an indeterminable number of interacting reflexes and drives processed within the brainstem and spinal cord.

The current analytical approach complements the traditional methods of quantifying the number and size of integrated bursts by providing information about specific neuronal recruitment patterns. Also, the current approach complements the assessment of single neurones, which quantifies how individual neurones behave once recruited (but they must be present during the search phase of the experiment), with information about how populations of neurones (within the recording field of the electrode) behave between varying levels of sympathetic activation. Thus, limitations of the current approach are that the size of that recording field is not known and that information about single neurones' behaviour cannot be provided.

In conjunction with previous single-unit analyses, the data from the current study enhance our understanding of how the sympathetic nervous system is activated during chemoreflex stress. This information leads to new possibilities to address long-standing questions that include (1) what reflex-specific recruitment strategies may exist in postganglionic sympathetic nerves, (2) how such patterns may be related to vasomotor control, and (3) the malleability of sympathetic neuronal properties and recruitment in health and disease.

Appendix I. Reliability of action potential detection

The reliability of the action potential detection method was tested by adding physiological action potential templates to a section of the real filtered MSNA signal and subsequently calculating the percentage of correct detection of these digitally added waveforms. This simulation was performed on data from two subjects that provided the highest (4.5) and lowest (3.8) SNRs in the current study. One minute of baseline MSNA signal was selected from each subject. In total, 12 bursts of sympathetic activity were found in the first subject and 20 bursts in the second subjects. Two different physiological action potential templates based on mean action potential waveforms were constructed and 20 individual 'action potentials' were randomly added to each sympathetic burst. In total 240 (i.e. 20×12 bursts) and 400 (i.e. 20×20 bursts) action potential waveforms were inserted randomly into sympathetic bursts in each period of real baseline data (see online Supplemental Material, Supplemental Fig. 1). The new matched wavelet action potential detector method was then used to detect the location and size of these added action potentials and the percentage of correct detection was calculated. The experiment was repeated 100 separate times and in each trial a different random placement of action potentials was used.

The mean percentage of correct detection of action potentials was $98.6 \pm 1.3\%$ for the signal with the highest SNR (4.5) and $88.7 \pm 2.5\%$ for signal with the lowest SNR (3.8). A complete performance analysis of the matched wavelet method using a simulated MSNA signal with a

different set of burst rate, action potential rate and SNRs has also been reported previously by Salmanpour *et al.* (2010).

Appendix II. Determination of action potential morphology before amplification and band-pass filtering (i.e. at the recording electrode)

It is possible to estimate the effect of amplification and band-pass filtering on a recorded action potential's morphology. To this end, the delay created by the band-pass filter was computed. Subsequently, an algorithm was produced (see Supplemental Fig. 2*B*, steps 1–3) that corrected each action potential's position. Once the position of the detected peaks was computed, a discriminator algorithm extracted each action potential waveform from the signal before the band pass filter. An average of all extracted action potentials was calculated, representing the mean action potential morphology before the band-pass filter (see Supplemental Fig. 2*B*, steps 5 and 6). To discover the raw action potential waveform before it is modified by the pre-amplifier and variable gain amplifier, the total transfer function for all of the amplifiers (pre-amplifiers, isolation-amplifier and variable gain amplifier) was calculated. Then, the discrete Fourier transform (DFT) of the averaged pattern before the band-pass filtering was multiplied by the inverse of the total transfer function of the amplifiers. This process produced the DFT of the averaged action potential waveform before the pre-amplifier. By taking the inverse DFT of this averaged waveform, the real action potential morphology was determined in the time domain (see Supplemental Fig. 2*B*, step 7). As shown in Supplemental Fig. 2*B*, the mean action potential waveform at the recording electrode has a major negative peak (Step 7).

References

Andresen MC & Yang M (1989). Interaction among unitary spike trains: implications for whole nerve measurements. *Am J Physiol Regul Integr Comp Physiol* **256**, R997–1004.

Ashley C, Burton D, Sverrisdottir YB, Sander M, McKenzie D & Macefield VG (2010). Firing probability and mean firing rates of human muscle vasoconstrictor neurones are elevated during chronic asphyxia. *J Physiol* **588**, 701–711.

Chad D, Shoukimas GM, Bradley WG, Bosch EP, Shahani BT & Young RR (1981). Peripheral nerve unmyelinated axons following lumbar sympathectomy. *Ann Neurol* **10**, 486–488.

Clamann HP & Henneman E (1976). Electrical measurement of axon diameter and its use in relating motoneuron size to critical firing level. *J Neurophysiol* **39**, 844–851.

Delius W, Hagbarth KE, Hongell A & Wallin BG (1972). Manoeuvres affecting sympathetic outflow in human muscle nerves. *Acta Physiol Scand* **84**, 82–94.

Diedrich A, Charoensuk W, Brychta RJ, Ertl AC & Shiavi R (2003). Analysis of raw microneurographic recordings based on wavelet de-noising technique and classification algorithm: wavelet analysis in microneurography. *IEEE Trans Biomed Eng* **50**, 41–50.

Elam M, McKenzie D & Macefield V (2002). Mechanisms of sympathoexcitation: single-unit analysis of muscle vasoconstrictor neurons in awake OSAS subjects. *J Appl Physiol* **93**, 297–303.

Fagius J & Wallin BG (1980). Sympathetic reflex latencies and conduction velocities in normal man. *J Neurol Sci* **47**, 433–448.

Grundfest H & Gasser HS (1938). Properties of mammalian nerve fibers of slowest conduction. *Am J Physiol* **123**, 307–318.

Hagbarth KE & Vallbo AB (1968). Pulse and respiratory grouping of sympathetic impulses in human muscle-nerves. *Acta Physiol Scand* **74**, 96–108.

Henneman E, Somjen G & Carpenter DO (1965). Functional significance of cell size in spinal motoneurons. *J Neurophysiol* **28**, 560–580.

Hinkle DE, Wiersma W & Jurs SG (2003). Multiple-comparison procedures. In *Applied Statistic for the Behavioral Sciences*, pp. 370–399. Houghton Mifflin Company, New York.

Jacobs JM & Love S (1985). Qualitative and quantitative morphology of human sural nerve at different ages. *Brain* **108**, 897–924.

Johnstone IM & Silverman BW (1997). Wavelet threshold estimators for data with correlated noise. *J R Statist Soc* **59**, 319–351.

Kienbaum P, Karlssonn T, Sverrisdottir YB, Elam M & Wallin BG (2001). Two sites for modulation of human sympathetic activity by arterial baroreceptors? *J Physiol* **531**, 861–869.

Lambert E, Straznicky N, Schlaich M, Esler M, Dawood T, Hotchkin E & Lambert G (2007). Differing pattern of sympathoexcitation in normal-weight and obesity-related hypertension. *Hypertension* **50**, 862–868.

Macefield VG & Elam M (2004). Comparison of the firing patterns of human postganglionic sympathetic neurones and spinal α motoneurones during brief bursts. *Exp Physiol* **89**, 82–88.

Macefield VG, Rundqvist B, Sverrisdottir YB, Wallin BG & Elam M (1999). Firing properties of single muscle vasoconstrictor neurons in the sympathoexcitation associated with congestive heart failure. *Circulation* **100**, 1708–1713.

Macefield VG & Wallin BG (1999). Firing properties of single vasoconstrictor neurones in human subjects with high levels of muscle sympathetic activity. *J Physiol* **516**, 293–301.

Macefield VG, Wallin BG & Vallbo AB (1994). The discharge behaviour of single vasoconstrictor motoneurones in human muscle nerves. *J Physiol* **481**, 799–809.

Malpas SC, Bendle RD, Head GA & Ricketts JH (1996). Frequency and amplitude of sympathetic discharges by baroreflexes during hypoxia in conscious rabbits. *Am J Physiol Heart Circ Physiol* **271**, H2563–H2574.

McKeon B & Burke D (1981). Component of muscle spindle discharge related to arterial pulse. *J Neurophysiol* **46**, 788–796.

Meckler RL & Weaver LC (1988). Characteristics of ongoing and reflex discharge of single splenic and renal sympathetic postganglionic fibres in cats. *J Physiol* **396**, 139–153.

Murai H, Takamura M, Maruyama M, Nakano M, Ikeda T, Kobayashi D, Otowa K, Ootsuji H, Okajima M, Furusho H, Takata S & Kaneko S (2009). Altered firing pattern of single-unit muscle sympathetic nerve activity during handgrip exercise in chronic heart failure. *J Physiol* **587**, 2613–2622.

Salmanpour A, Brown LJ & Shoemaker JK (2010). Spike detection in human muscle sympathetic nerve activity using a matched wavelet approach. *J Neurosci Methods* (in press).

Scott DW (1979). On optimal and data-based histograms. *Biometrika* **66**, 605–610.

Spickler JW & Kezdi P (1969). Probability of spike summations in baroreceptor electroneurograms. *J Appl Physiol* **27**, 919–922.

Steinback CD, Salzer D, Medeiros PJ, Kowalchuk J & Shoemaker JK (2009). Hypercapnic vs. hypoxic control of cardiovascular, cardiovagal, and sympathetic function. *Am J Physiol Regul Integr Comp Physiol* **296**, R402–R410.

Tsukahara R & Mano T (1997). The recruitment pattern of single vasoconstrictor neurons in human. *J Auton Nerv Syst* **66**, 26–34.

Wallin BG (1993). Assessment of sympathetic mechanisms from recordings of postganglionic efferent nerve traffic. In *Cardiovascular Reflex Control in Health and Disease*, ed. Hainsworth R & Mark AL, pp. 65–93. W.B. Saunders Company Ltd, London.

Wallin BG, Burke D & Gandevia S (1994). Coupling between variations in strength and baroreflex latency of sympathetic discharges in human muscle nerves. *J Physiol* **474**, 331–338.

Westgaard RH & De Luca CJ (2001). Motor control of low-threshold motor units in the human trapezius muscle. *J Neurophysiol* **85**, 1777–1781.

Xie A, Skatrud JB, Puleo DS & Morgan BJ (1999). Arousal from sleep shortens sympathetic burst latency in humans. *J Physiol* **515**, 621–628.

Author contributions

Data for the current manuscript were collected in the laboratory of Z.D. Authors contributed as follows: conception and design of study: C.D.S. and J.K.S.; development of the multi-unit analysis algorithm: A.S.; data collection, analysis, and interpretation: C.D.S., A.S., T.B., Z.D. and J.K.S. drafting of manuscript: C.D.S.; critical review of manuscript prior to publication: C.D.S., A.S., T.B., Z.D. and J.K.S. The authors declare no competing financial interests.

Acknowledgements

The authors would like to thank Ivana Banic, Dr Dubravka Glucina, Dr Jasenka Kraljevic, and Dr Petra Zubin for their assistance in data collection. This study was funded by the Croatian Ministry of Science, Education and Sports grant no. 216-2160133-0130 to Z.D., and by the Natural Sciences and Engineering Research Council of Canada (NSERC) to J.K.S. C.D.S. was supported by a NSERC Alexander Graham Bell Canadian Graduate Scholarship and a NSERC Michael Smith Foreign Study Scholarship.